

Boundary Layer Flow of Dusty Ferrofluid: A Comparative Analysis of Stagnation Flow Influence

Cik Siti Hajar Abdulah¹, Rohana Abdul Hamid^{1,2,*}, Roslinda Nazar³

¹ Institute of Engineering Mathematics, Universiti Malaysia Perlis (UniMAP), 02600 Arau, Perlis, Malaysia.

² Centre of Excellence for Social Innovation and Sustainability (CoESIS), Universiti Malaysia Perlis (UniMAP), 02600 Arau, Perlis, Malaysia.

³ Department of Mathematical Sciences, Faculty of Science & Technology, Universiti Kebangsaan Malaysia, 43600 UKM Bangi, Selangor, Malaysia.

*Corresponding author : rohanahamid@unimap.edu.my

Received: 26 September 2023

Revised: 23 July 2024

Accepted: 27 September 2024

ABSTRACT

This research examines the characteristics of the boundary layer in the occurrence of dust particles within the ferrofluid boundary layer, aiming to understand the impact of stagnation flow or without stagnation flow in such systems. For this purpose, ferroparticles, namely magnetite (Fe_3O_4), are taken into consideration with kerosene and water as base fluids. The governing partial differential equations of the problem under consideration are converted into ordinary differential equations (ODEs) through the utilization of similarity transformations. Here, the equations obtained are then numerically solved utilizing MATLAB's built-in `bvp4c` solver. Moreover, the parameters' effects, namely the dust particle loading, volume fraction of ferroparticles, and Eckert number to the flow with and without stagnation flow are computed and shown through tables and graphs. The findings indicate that the skin friction coefficient values for the stagnation-point flow are higher than those without stagnation-point flow. The Eckert number increases temperature profiles for both flows but more prominent in the flow without stagnation-point.

Keywords: Boundary layer, dusty ferrofluid, magnetohydrodynamics, moving surface, stagnation-point.

1 INTRODUCTION

Stagnation flow, also known as stagnation-point flow or zero-velocity flow, is a form of fluid flow in which the velocity of the fluid is zero at a specified point in the flow field. Moreover, the fluid comes to a full stop at the stagnation-point, resulting in a high-pressure area. The significance of stagnation flow may be seen in its application to fluid dynamics and aerodynamics [1]. For example, in gas turbines or jet engines, the stagnation pressure is used to measure the total energy of the entering air, which is critical for combustion and power generation [2]. Stagnation flow is essential for understanding the lift and drag forces experienced by objects moving through a fluid [3]. The stagnation-point on an airfoil or wing is the point at which the flow separates, resulting in changes in

pressure distribution and the formation of lift. By analysing stagnation flow, it can increase the performance and efficiency of aircraft wings, propellers, and other aerodynamic surfaces [4].

Numerous researchers have examined the stagnation flow towards a shrinking or stretching sheet. For instance, Rosali et al. [5] explored the stagnation-point flow as well as heat transfer in a porous media over a shrinking and stretching sheet. Lok et al. [6] examined the steady axisymmetric stagnation flow with respect to a viscous fluid on a vertical cylinder that can either stretch or shrink. Additionally, Bhattacharyya [7] further studied heat transfer concerning an unsteady boundary layer stagnation-point flow over a stretching or shrinking sheet. Lok and Pop [8] conducted extensive research on the unsteady separated stagnation-point flow over a stretching or shrinking sheet. Numerous researchers, including Yacob et al. [2], Bachok et al. [3], Bachok et al. [9], Aman et al. [10] and Sharma et al. [11] have also explored the flow towards stretching or shrinking sheets, considering various aspects. However, a significant limitation of these studies is that they do not consider the effects of dusty particles.

Presently, significant focus is placed by researchers on exploring the stagnation flow over a shrinking and stretching sheet in nanofluids. This attention is driven by its notable importance in engineering processes, including paper production, glass fiber production, hot rolling, wire drawing as well as glass blowing [12]. Siddiq et al. [13] studied the hydromagnetic radiative stagnation-point flow over a shrinking sheet of micropolar nanofluid, wherein the increment in thermophoretic and Brownian motion parameter values leads to reverse effects on the nanoparticle volume fraction. Jalilpour et al. [14] discovered a steady stagnation flow with heat transfer of a nanofluid toward a stretching surface, considering the influence of thermal radiation. The authors observed that reducing the local Nusselt number led to an increment in the thermophoresis parameter as well as Brownian motion parameter. Apart from that, Kameswaran et al. [15] further investigated the impact of homogeneous-heterogeneous reactions on the stagnation-point flow of a nanofluid over a stretching or shrinking sheet.

Based on previous research, the authors were motivated to investigate the stagnation flow of dusty ferrofluid, an area that remains largely unexplored. To the authors' knowledge, no existing studies have examined the stagnation flow of dusty ferrofluid over stretching or shrinking surfaces using the current formulation. Therefore, the primary objective of this study is to fill this research gap by thoroughly analyzing the stagnation flow of dusty ferrofluid and conducting a comparative analysis with the findings of Hamid et al. [16], which did not include stagnation flow. The relevance of this study lies in its potential to enhance the understanding of dusty ferrofluids in various industrial applications, particularly in processes involving heat transfer and fluid dynamics. Furthermore, outstanding numerical results were generated for this study utilizing the `bvp4c` function in MATLAB, demonstrating the effectiveness of the proposed formulation.

2 MATHEMATICAL FORMULATION

A laminar boundary layer stagnation-point flow of ferrofluid containing dust particles over a moving flat surface. The free stream velocity is expressed as $U_e(x)$ while the surface is moving with velocity $U_w(x)$. The ferrofluid is assumed to contain magnetic nanoparticles, viscous dissipation, and an external magnetic field of strength B_0 is implemented normal to the surface. In this study, we closely

followed the formulation presented in Hamid et al. [16], including the stagnation flow. Hence, this problem's governing equations are as follows:

For ferrofluid phase

$$\frac{\partial u}{\partial x} + \frac{\partial v}{\partial y} = 0 \quad (1)$$

$$u \frac{\partial u}{\partial x} + v \frac{\partial u}{\partial y} = u_e \frac{\partial u_e}{\partial x} + v_{ff} \frac{\partial^2 u}{\partial y^2} - \frac{\sigma_{ff} B_0^2}{\rho_{ff}} (u - u_e) + \frac{\rho_p K}{\rho_{ff} m} (u_p - u) \quad (2)$$

$$u \frac{\partial T}{\partial x} + v \frac{\partial T}{\partial y} = \alpha_{ff} \frac{\partial^2 T}{\partial y^2} + \frac{\rho_p K}{(\rho c_p)_{ff} m} (u_p - u)^2 + \frac{\mu_{ff}}{(\rho c_p)_{ff}} \left(\frac{\partial u}{\partial y} \right)^2 + \frac{\rho_p c_m}{(\rho c_p)_{ff}} \frac{1}{\tau_T} (T_p - T) \quad (3)$$

For dust phase

$$\frac{\partial u_p}{\partial x} + \frac{\partial v_p}{\partial y} = 0 \quad (4)$$

$$u_p \frac{\partial u_p}{\partial x} + v_p \frac{\partial u_p}{\partial y} = \frac{K}{m} (u - u_p) \quad (5)$$

$$u_p \frac{\partial T_p}{\partial x} + v_p \frac{\partial T_p}{\partial y} = \frac{1}{\tau_T} (T - T_p) \quad (6)$$

subject to the boundary conditions

$$u = U_w(x), \quad v = V_w, \quad T = T_w(x) \quad \text{at } y = 0$$

$$u \rightarrow U_e(x), \quad u_p \rightarrow U_e(x), \quad v_p \rightarrow v, \quad T \rightarrow T_\infty, T_p \rightarrow T_\infty \quad \text{at } y \rightarrow \infty \quad (7)$$

This study uses the method of similarity transformation where the equations (1) - (6) with boundary condition (7) are reduced to ordinary differential equations.

$$u = axf'(\eta), \quad v = -\sqrt{av_f} f(\eta), \quad \eta = \sqrt{a/v_f} y$$

$$u_p = axF'(\eta), \quad v_p = -\sqrt{av_f} F(\eta), \quad \theta(\eta) = \frac{T - T_\infty}{T_w - T_\infty}, \quad \theta_p(\eta) = \frac{T_p - T_\infty}{T_w - T_\infty} \quad (8)$$

we define the parameters as follows [15]

$$U_e(x) = ax, \quad U_w(x) = cx, \quad T_w(x) = T_\infty + bx^2, \quad V_w = -s\sqrt{av_f}$$

$$\nu_{ff} = \frac{\mu_{ff}}{\rho_{ff}}, \quad \mu_{ff} = \frac{\mu_f}{(1-\phi)^{2.5}}, \quad \rho_{ff} = (1-\phi)\rho_f + \phi\rho_s,$$

$$\alpha_{ff} = \frac{k_{ff}}{(\rho c_p)_{ff}}, \quad (\rho c_p)_{ff} = (1-\phi)(\rho c_p)_f + \phi(\rho c_p)_s, \quad (9)$$

Using transformation (8) and equations in (9) into equations (1) – (6), we obtain the following:

$$\frac{1}{(1-\phi)^{2.5} \varepsilon_1} f'''' + f f'' - f'^2 - \frac{\varepsilon_2}{\varepsilon_1} M(f' - 1) + \frac{1}{\varepsilon_1} l \beta (F' - f') + 1 = 0 \quad (10)$$

$$\frac{1}{Pr \varepsilon_4} \theta'' + f \theta' - 2f' \theta + \frac{1}{\varepsilon_4} l Ec \beta (F' - f')^2 + \frac{1}{(1-\phi)^{2.5} \varepsilon_4} Ec (f'')^2 + \frac{1}{\varepsilon_4} l \zeta \beta_T (\theta_p - \theta) = 0 \quad (11)$$

$$FF'' - F'^2 + \beta (f' - F') = 0 \quad (12)$$

$$F \theta_p' - 2F' \theta_p + \beta_T (\theta - \theta_p) = 0 \quad (13)$$

with boundary condition

$$f(0) = s, \quad f'(0) = \lambda, \quad \theta(0) = 1,$$

$$f'(\eta) \rightarrow 1, \quad F'(\eta) \rightarrow 1, \quad F(\eta) \rightarrow f(\eta), \quad \theta(\eta) \rightarrow 0, \quad \theta_p(\eta) \rightarrow 0 \quad \text{as } \eta \rightarrow \infty \quad (14)$$

in which

$$\varepsilon_1 = (1-\phi) + \phi(\rho_s / \rho_f), \quad \varepsilon_2 = \frac{\sigma_{ff}}{\sigma_f} = 1 + \frac{3(\frac{\sigma_s}{\sigma_f} - 1)\phi}{(\frac{\sigma_s}{\sigma_f} + 2) - (\frac{\sigma_s}{\sigma_f} - 1)\phi}$$

$$\varepsilon_3 = \frac{k_{ff}}{k_f} = \frac{k_s + 2k_f - 2\phi(k_f - k_s)}{k_s + 2k_f + \phi(k_f - k_s)}, \quad \varepsilon_4 = (1-\phi) + \phi \frac{(\rho c_p)_s}{(\rho c_p)_f}, \quad (15)$$

in which l expresses the dust particle loading, β expresses the fluid-dust interaction parameter, M expresses the magnetic field parameter, Pr expresses the Prandtl number, ζ expresses the specific heat parameter, β_T refers to the fluid-dust interaction parameter for temperature, s expresses the suction parameter ($s > 0$), Ec refers to the Eckert number, λ refers to the shrinking ($\lambda < 0$) as well as stretching ($\lambda > 0$) parameter. Moreover, ρ implies the density while σ expresses the electrical conductivity as well as C_p refers to the fluid-phase specific heat.

The parameters $l, \beta, M, Pr, \zeta, \beta_T$ and Ec are defined by:

$$l = \frac{\rho_p}{\rho_f}, \beta = \frac{K}{ma}, M = \frac{\sigma_f B_0^2}{a\rho_f}, Pr = \frac{\nu_f}{\alpha_f}, \zeta = \frac{c_m}{(c_p)_f},$$

$$\beta_T = \frac{1}{a\tau_T}, Ec = \frac{a^2}{b(c_p)_f} \quad (16)$$

Moreover, the physical characteristics essential in the current problem are the local Nusselt number Nu_x as well as skin friction coefficient C_f , expressed as

$$C_f = \frac{\tau_w}{\rho_f U_e^2(x)}, Nu_x = \frac{xq_w}{k_f(T_w - T_\infty)} \quad (17)$$

The surface heat flux q_w and the shear stress τ_w at the shrinking/stretching surface $y=0$ are expressed by:

$$\tau_w = \mu_{ff} \left(\frac{\partial u}{\partial y} \right)_{y=0}, q_w = -k_{ff} \left(\frac{\partial T}{\partial y} \right)_{y=0} \quad (18)$$

Therefore, the dimensionless wall shear stress $C_f Re_x^{1/2}$ as well as the dimensionless heat flux $Nu_x Re_x^{-1/2}$ are expressed as

$$C_f Re_x^{1/2} = \frac{f''(0)}{(1-\phi)^{2.5}}, Nu_x Re_x^{-1/2} = -\frac{k_{ff}}{k_f} \theta'(0) \quad (19)$$

where $Re_x = U_e(x)x / \nu_f$.

Table 1 : Thermophysical properties of water [17], kerosene [8] and Fe_3O_4

Properties	Water	Kerosene	Fe_3O_4
$\rho(kg / m^3)$	997.1	780	5180
$c_p(J / kgK)$	4179	2090	670
$k(W / mK)$	0.613	0.149	9.7
$\sigma(\Omega m)^{-1}$	0.05	6×10^{-10}	25 000
Pr	6.2	21	-

3 RESULTS AND DISCUSSION

We solve the differential equations (1)- (6) subject to the boundary condition equation (7) numerically by employing some similarity transformations. Numerical values are iteratively approximated by using the MATLAB built-in bvp4c solver with thermophysical properties in Table 1. To validate the solutions, we make a comparison the numerical findings with the existence study of Hamid et al. [16] for the case without stagnation point flow. Here, the comparisons are indicated in Table 2 for the skin friction coefficient $-C_f Re_x^{1/2}$ values. It is clear that the values obtained from this study aligns very well with the resulted reporter by Hamid et al.[16]. Hence, it can be presumed that the current numerical method can be used with certain precision for this problem.

Table 2: Comparison $-C_f Re_x^{1/2}$ values when $\phi = 0, s = 2$ and $\lambda = 1$

l	β	M	Hamid et al.[16]	Present results
0.2	0.02	3	3.236960	3.236960
		5	3.646505	3.646505
	0.5	3	3.256936	3.256936
		5	3.663519	3.663519
1	0.02	3	3.240524	3.240524
		5	3.649519	3.649519
	0.5	3	3.338681	3.338681
		5	3.733518	3.733518

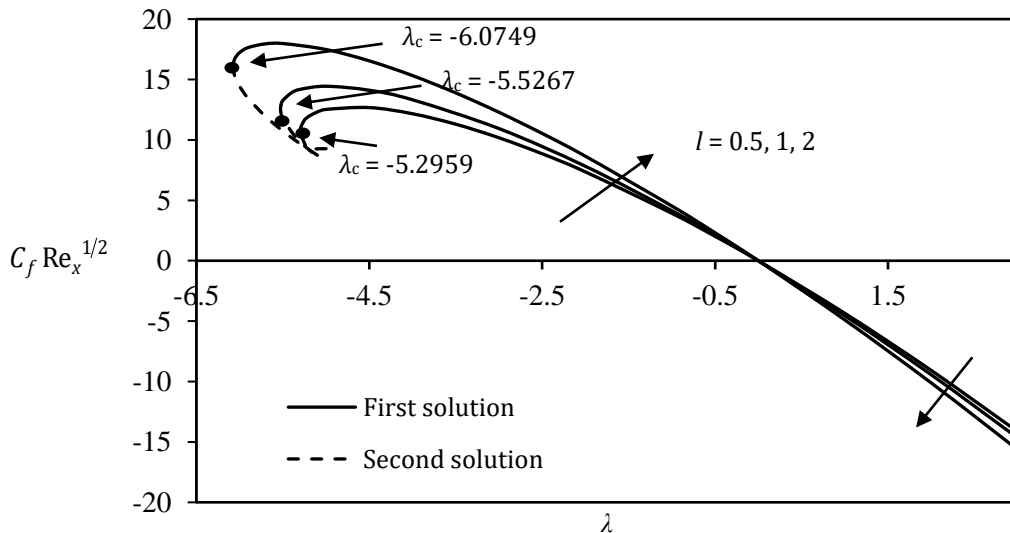


Figure 1: Variation of the skin friction of Fe_3O_4 for distinct values of l when $\beta = 2.5, M = 3, \phi = 0.01$ for water-based ferrofluid (Hamid et al.[16] – without stagnation-point flow)

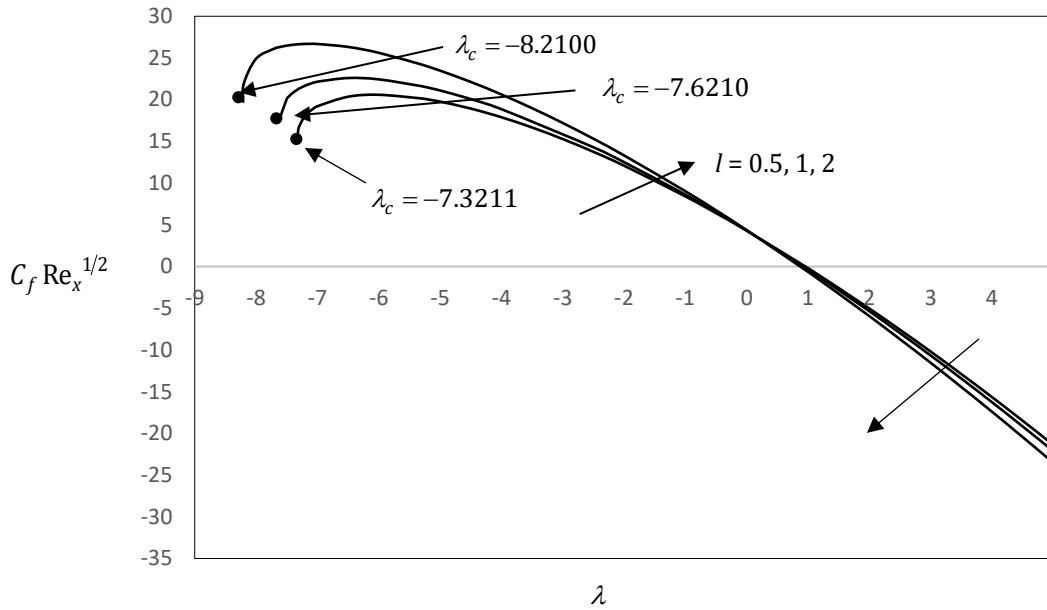


Figure 2: Variation of the skin friction of Fe_3O_4 for distinct values of l when $\beta = 2.5, M = 3, s = 3$ and $\phi = 0.01$ for water-based ferrofluid (present study – with stagnation-point flow)

Figures 1 and 2 show the variation of the skin friction coefficient, $C_f Re_x^{1/2}$ of Fe_3O_4 for various values of dust particle loading (l) when $\beta = 2.5, M = 3, s = 3$ and $\phi = 0.01$ for water-based ferrofluid. Fig. 1 shows the skin friction coefficient without stagnation flow, wherein we can observe the second solution in the shrinking region. On the other hand, Fig. 2 illustrates the skin friction coefficient with the stagnation flow, but unfortunately, the second solution cannot be found in this case. In both figures, as the number of dust particle loading increases on the stretching surface ($\lambda > 0$), the skin friction coefficient decreases. However, for shrinking surface ($\lambda < 0$), when dust particle loading increases, the skin friction also increases. This finding is relevant in applications where surface drag plays a significant role, such as in the design of magnetic fluid seals and enhanced oil recovery systems, where controlling friction is key to improving performance. Notably, Fig. 2 demonstrates that the problem of stagnation flow has a higher range of solutions.

Table 3: Values of $-C_f Re_x^{1/2}$ of Fe_3O_4 ferroparticles when $s = 3, l = 0.5$ without stagnation (Hamid et al.[16])

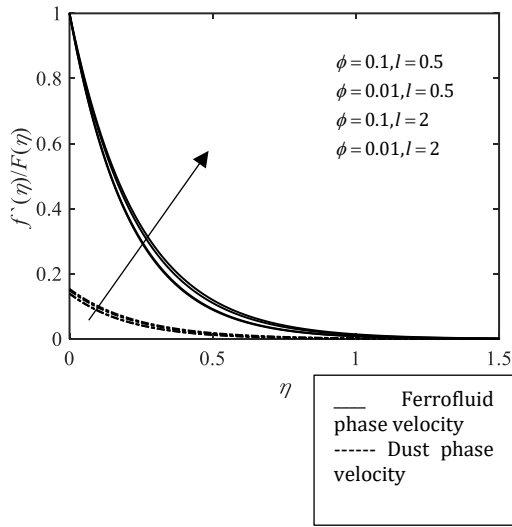
Base fluid	ϕ	$M = 0$			$M = 3$			
		$\beta = 0$	$\beta = 0.2$	$\beta = 2.5$	$\beta = 0$	$\beta = 0.2$	$\beta = 2.5$	
$\lambda = 1$ (stretching)	Water	0.01	3.436869	3.463543	3.700573	4.147644	4.167111	4.349512
		0.05	3.975314	4.001011	4.232730	4.750121	4.769141	4.948892
		0.1	4.655414	4.680609	4.910182	5.533143	5.551934	5.730613
	Kerosene	0.01	3.480589	3.506963	3.742042	4.185358	4.204708	4.386304
		0.05	4.193746	4.218235	4.441696	4.940466	4.958984	5.135135
		0.1	5.092073	5.115303	5.330968	5.916208	5.934143	6.106554

$\lambda = -1$ (shrinking)	Water	0.01	2.736450	2.778025	3.097117	3.694561	3.718007	3.924881
		0.05	3.200318	3.239601	3.550388	4.236734	4.259644	4.464179
		0.1	3.769138	3.807282	4.115288	4.938512	4.961147	5.164922
	Kerosene	0.01	2.780578	2.821437	3.137167	3.728748	3.752064	3.958244
		0.05	3.420528	3.457061	3.753652	4.410995	4.433322	4.634537
		0.1	4.209004	4.242813	4.526879	5.291389	5.313016	5.510768

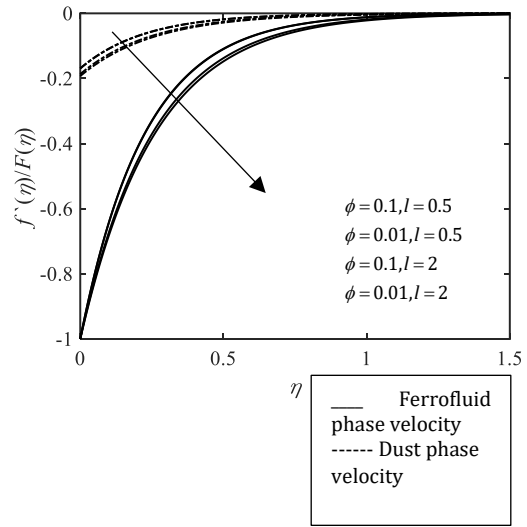
Table 4: Values of $-C_f Re_x^{1/2}$ of Fe_3O_4 ferroparticles when $s = 3, l = 0.5$ with stagnation (present study)

Base fluid	ϕ	$M = 0$			$M = 3$			
		$\beta = 0$	$\beta = 0.2$	$\beta = 2.5$	$\beta = 0$	$\beta = 0.2$	$\beta = 2.5$	
$\lambda = 1$ (stretching)	Water	0.01	0.000000	0.033381	0.257018	0.000000	0.023385	0.180451
		0.05	0.000000	0.033312	0.259028	0.000000	0.023461	0.182088
		0.1	0.000000	0.033296	0.261485	0.000000	0.023522	0.183678
	Kerosene	0.01	0.000000	0.033350	0.256953	0.000000	0.023430	0.180852
		0.05	0.000000	0.033180	0.258672	0.000000	0.023650	0.183809
		0.1	0.000000	0.033077	0.260728	0.000000	0.023839	0.186572
$\lambda = -1$ (shrinking)	Water	0.01	6.801708	6.811366	7.023271	8.206200	8.217864	8.415806
		0.05	7.872622	7.880710	8.079133	9.402297	9.412996	9.603379
		0.1	9.222656	9.229906	9.420547	10.954738	10.964912	11.151122
	Kerosene	0.01	6.889646	6.898839	7.106943	8.281854	8.293230	8.488995
		0.05	8.311780	8.318010	8.500632	9.784319	9.793793	9.974584
		0.1	10.100325	10.104577	10.269035	11.723749	11.731860	11.901549

Tables 3 and 4 display the skin friction coefficient $-C_f Re_x^{1/2}$ variations for distinct values of volume fraction of solid ferroparticle (ϕ), magnetic field (M), as well as fluid-dust interaction parameter (β) in two base fluids, kerosene and water. Table 3 presents the skin friction values for the problem without stagnation-point flow, whereas Table 4 shows the skin friction values for the problem with stagnation-point flow. It should be note that negative values of $C_f Re_x^{1/2}$ indicate that the ferrofluid applying drag force in the opposite direction with respect to the surface motion. Moreover, Table 3 reveals that the skin friction coefficient increases with the increment in the values of ϕ , M and β . Conversely, in Table 4, the skin friction shows a decrease as M increases, while the other parameters follow a similar trend. This information is crucial for optimizing the design of systems like heat exchangers and ferrofluid-based dampers, where surface friction needs to be minimized for increased efficiency. Thus, it is obvious from both tables that the problem of stagnation flow yields the lowest values of $C_f Re_x^{1/2}$ when the surface is stretched ($\lambda = 1$). Conversely, the highest skin friction coefficients are recorded when the surface is shrunk ($\lambda = -1$). It is possible that when the surface is shrinking, the fluid flow is slowing down, causing more resistance and higher friction.

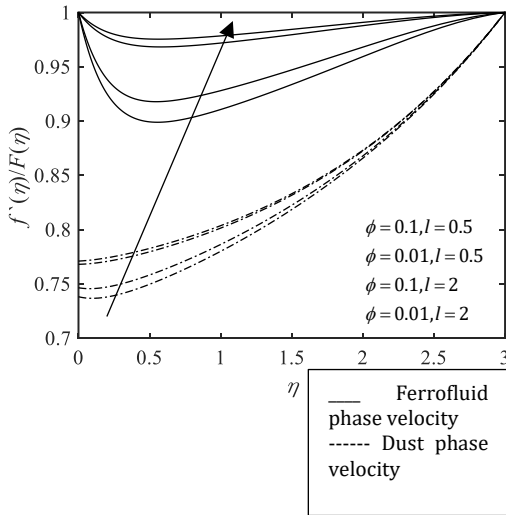


Stretching ($\lambda = 1$)

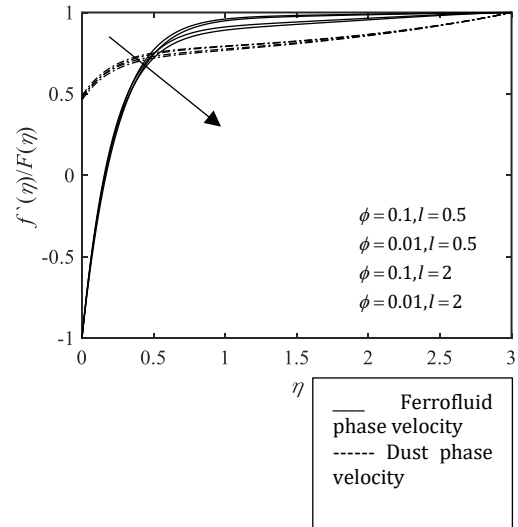


Shrinking ($\lambda = -1$)

a) Without stagnation (Hamid et al.[16])



Stretching ($\lambda = 1$)



Shrinking ($\lambda = -1$)

b) With stagnation (Present study)

Figure 3: Dust phase and ferrofluid phase velocity profiles for various values of parameter l and ϕ for $M = 3$ and $\beta = 2.5$ for water-based ferrofluid.

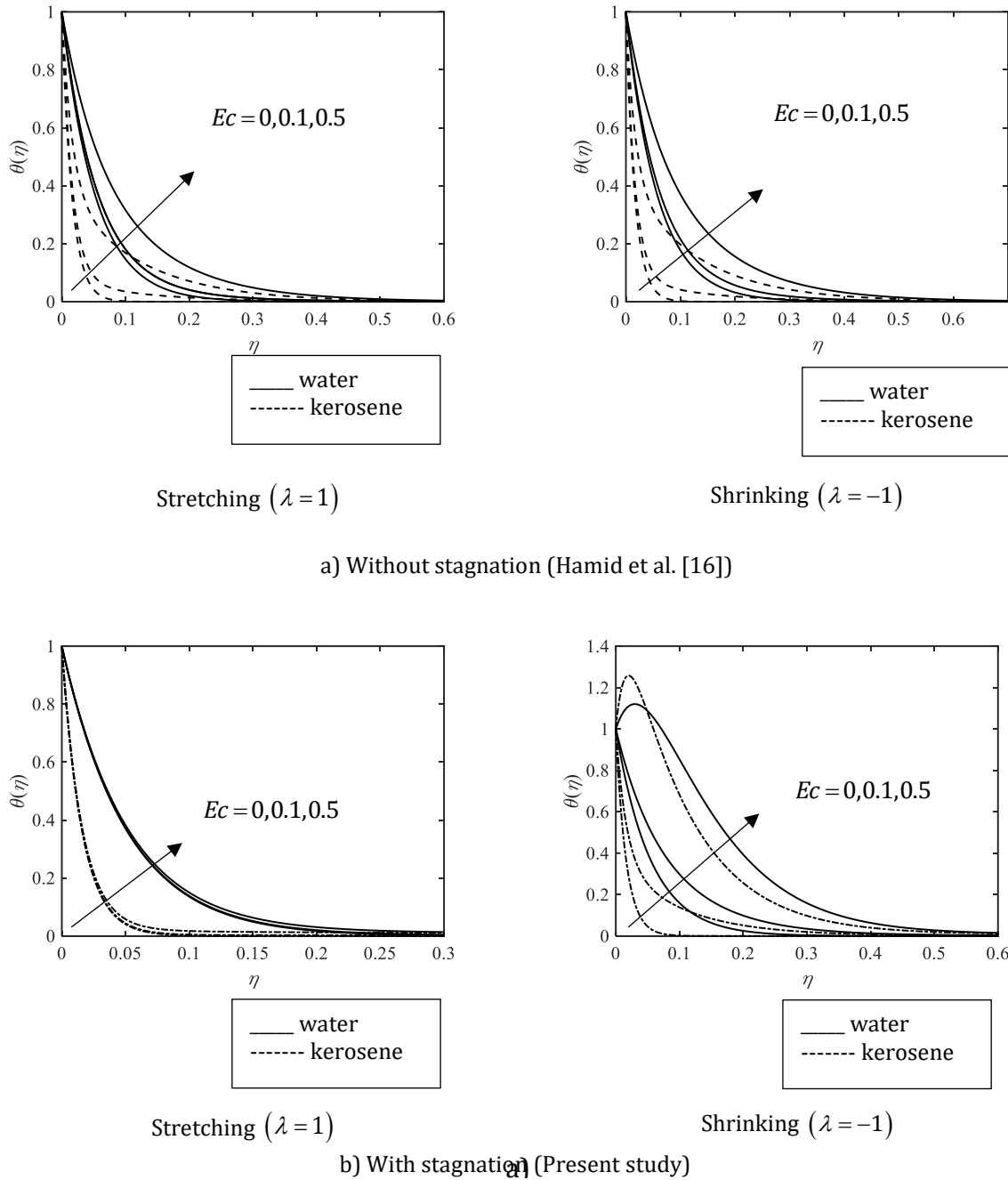


Figure 4: Ferrofluid phase temperature profiles for different Ec values and base fluid for $M = 3, \phi = 0.01, s = 3$ and $\beta_T = 2.5$

Figures 3(a) and 3(b) illustrate the velocity profiles of the dust phase and ferrofluid phase having different volume fraction of solid ferroparticles (ϕ) and dust particle loading (l). In both Figs. 3(a) and 3(b), without stagnation flow and with stagnation for stretching/shrinking surface, it may be seen that both phases' velocity rises as the volume fraction of solid ferroparticles decreases and dust loading particle increases. It is possible, therefore, with fewer solid ferroparticles present, there is

less interaction and hindrance to the flow, allowing the phases to move more freely and at higher velocities. Meanwhile, the presence of dust particles can increase the flow disturbances, which eventually increase the velocities. This result can be applied to optimize the flow velocity in industrial processes like ferrofluid cooling systems and magnetic fluid transportation, where higher velocity may improve system performance.

Figure 4 illustrates the ferrofluid phase temperature profiles for various Eckert number, Ec values with kerosene as well as water as the base fluid. Moreover, Eckert number denotes the kinetic energy to thermal energy ratio, quantifying the impact of viscous dissipation in the flow. Figure 4(a) shows the temperature profiles without stagnation flow and Fig. 4(b) with stagnation flow. It is seen that temperature profiles rise with the increment of Ec in both figures. However, it is apparent that the effect of Ec is more prominent for the problem with stagnation flow. When there is no stagnation flow, the fluid flows more freely over the surface. An increase in the Eckert number might lead to a higher ratio of kinetic energy to thermal energy, which could enhance the heat transfer. Meanwhile in stagnation flow, increased pressure and temperature at the stagnation-point might already dominate the heat transfer, and the contribution of the kinetic energy, which is influenced by the Eckert number might be comparatively smaller. Therefore, even with increase in the Eckert number, it may not significantly impact the already dominant heat transfer effects at the stagnation-point, causing a marginal rise in the temperature profiles.

4 CONCLUSION

The ferrofluid boundary layer with dust particles analysis has been investigated. The focus is to understand the influence of some parameters, including dust particle loading, volume fraction of ferroparticles, and Eckert number on the flow with stagnation or without stagnation-point. In order to accomplish this, similarity transformations are applied to convert the governing equations into ODEs. Subsequently, these transformed equations are numerically solved using MATLAB's built-in `bvp4c` solver.

The results reveal that the skin friction coefficient values for the stagnation-point flow are greater in comparison to the flow without a stagnation-point, especially in the scenario of the shrinking sheet. Furthermore, the Eckert number was found to increase the temperature profiles for both flows. However, its influence was more pronounced in the flow without stagnation-point. This implies that greater Eckert number values result in a more significant rise in the temperature profiles for the flow without stagnation, indicating a stronger coupling between kinetic energy and thermal energy in this case.

The outcomes of this study provide valuable contributions to the understanding of ferrofluid behavior in the presence of dust particles, particularly in flows with and without stagnation. These insights hold significant implications for various engineering applications involving ferrofluids, where heat transfer and fluid dynamics are critical factors.

The scope of this research can be expanded by incorporating more intricate boundary conditions, such as time-dependent stretching or shrinking surfaces and varying magnetic fields, to more closely simulate industrial processes. Further investigations could also examine the influence of various nanoparticle shapes, sizes, and types, as well as the behavior of non-Newtonian dusty ferrofluids,

thereby broadening the potential applications. Moreover, extending the analysis to account for turbulence effects and three-dimensional flow could provide deeper insights into the behavior of such systems under more realistic conditions.

The practical implications of this study are considerable, particularly in areas like cooling systems for electronic devices, where ferrofluids are used to regulate heat dissipation, and magnetic drug targeting, which requires precise control over fluid dynamics. By improving the ability to predict and manage temperature changes and skin friction in these fluids, this research can contribute to the development of more efficient designs for heat exchangers, magnetic fluid seals, and lubrication systems.

ACKNOWLEDGEMENT

The authors want to acknowledge the financial supports obtained from the Fundamental Research Grant Scheme (FRGS) under a grant number of FRGS/1/2020/STG06/UNIMAP/02/4 from the Ministry of Higher Education Malaysia and the Collaborative Research Grant (SST-2022-015) from the Universiti Kebangsaan Malaysia.

REFERENCES

- [1] K. Bhattacharyya, "Dual solutions in boundary layer stagnation-point flow and mass transfer with chemical reaction past a stretching/shrinking sheet," *Int. Commun. Heat Mass Transf.*, vol. 38, no. 7, pp. 917–922, 2011, doi: 10.1016/j.icheatmasstransfer.2011.04.020.
- [2] N. A. Yacob, A. Ishak, and I. Pop, "Melting heat transfer in boundary layer stagnation-point flow towards a stretching/shrinking sheet in a micropolar fluid," *Comput. Fluids*, vol. 47, no. 1, pp. 16–21, 2011, doi: 10.1016/j.compfluid.2011.01.040.
- [3] N. Bachok, A. Ishak, and I. Pop, "Melting heat transfer in boundary layer stagnation-point flow towards a stretching/shrinking sheet," *Phys. Lett. Sect. A Gen. At. Solid State Phys.*, vol. 374, no. 40, pp. 4075–4079, 2010, doi: 10.1016/j.physleta.2010.08.032.
- [4] L. Müller, W. Heinze, D. Kožulović, M. Hepperle, and R. Radespiel, "Aerodynamic installation effects of an over-The-wing propeller on a high-lift configuration," *J. Aircr.*, vol. 51, no. 1, pp. 249–258, 2014, doi: 10.2514/1.C032307.
- [5] H. Rosali, A. Ishak, and I. Pop, "Stagnation point flow and heat transfer over a stretching/shrinking sheet in a porous medium," *Int. Commun. Heat Mass Transf.*, vol. 38, no. 8, pp. 1029–1032, 2011, doi: 10.1016/j.icheatmasstransfer.2011.04.031.
- [6] Y. Y. Lok, J. H. Merkin, and I. Pop, "Mixed convection flow near the axisymmetric stagnation point on a stretching or shrinking cylinder," *Int. J. Therm. Sci.*, vol. 59, pp. 186–194, 2012, doi: 10.1016/j.ijthermalsci.2012.04.008.

- [7] K. Bhattacharyya, "Heat transfer analysis in unsteady boundary layer stagnation-point flow towards a shrinking/stretching sheet," *Ain Shams Eng. J.*, vol. 4, no. 2, pp. 259–264, 2013, doi: 10.1016/j.asej.2012.07.002.
- [8] Y. Y. Lok and I. Pop, "Stretching or shrinking sheet problem for unsteady separated stagnation-point flow," *Meccanica*, vol. 49, no. 6, pp. 1479–1492, 2014, doi: 10.1007/s11012-014-9932-y.
- [9] N. Bachok, A. Ishak, and I. Pop, "Stagnation point flow toward a stretching/shrinking sheet with a convective surface boundary condition," *J. Franklin Inst.*, vol. 350, no. 9, pp. 2736–2744, 2013, doi: 10.1016/j.jfranklin.2013.07.002.
- [10] F. Aman, A. Ishak, and I. Pop, "Magnetohydrodynamic stagnation-point flow towards a stretching/shrinking sheet with slip effects," *Int. Commun. Heat Mass Transf.*, vol. 47, pp. 68–72, 2013, doi: 10.1016/j.icheatmasstransfer.2013.06.005.
- [11] R. Sharma, A. Ishak, and I. Pop, "Stability analysis of magnetohydrodynamic stagnation-point flow toward a stretching/shrinking sheet," *Comput. Fluids*, vol. 102, pp. 94–98, 2014, doi: 10.1016/j.compfluid.2014.06.022.
- [12] N. Bachok, A. Ishak, and I. Pop, "Stagnation-point flow over a stretching/shrinking sheet in a nanofluid," *Nanoscale Res. Lett.*, vol. 6, pp. 1–10, 2011, doi: 10.1186/1556-276X-6-623.
- [13] M. K. Siddiq, A. Rauf, S. A. Shehzad, F. M. Abbasi, and M. A. Meraj, "Thermally and solutally convective radiation in MHD stagnation point flow of micropolar nanofluid over a shrinking sheet," *Alexandria Eng. J.*, vol. 57, no. 2, pp. 963–971, 2018, doi: 10.1016/j.aej.2017.01.019.
- [14] B. Jalilpour, S. Jafarmadar, M. M. Rashidi, D. D. Ganji, R. Rahime, and A. B. Shotorban, "MHD non-orthogonal stagnation point flow of a nanofluid towards a stretching surface in the presence of thermal radiation," *Ain Shams Eng. J.*, vol. 9, no. 4, pp. 1671–1681, 2018, doi: 10.1016/j.asej.2016.09.011.
- [15] P. K. Kameswaran, P. Sibanda, C. R. Reddy, and P. Vsn Murthy, "Dual solutions of stagnation-point flow of a nanofluid over a stretching surface," *Bound. Value Probl.*, vol. 2013, pp. 1–12, 2013, doi: 10.1186/1687-2770-2013-188.
- [16] R. A. Hamid, R. Nazar, K. Naganthran, and I. Pop, "Dusty ferrofluid transport phenomena towards a non-isothermal moving surface with viscous dissipation," *Chinese J. Phys.*, vol. 75, 2022, doi: 10.1016/j.cjph.2021.11.002.
- [17] T. Hayat, S. Qayyum, M. Imtiaz, F. Alzahrani, and A. Alsaedi, "Partial slip effect in flow of magnetite-Fe₃O₄ nanoparticles between rotating stretchable disks," *J. Magn. Magn. Mater.*, vol. 413, pp. 39–48, 2016, doi: 10.1016/j.jmmm.2016.04.025.